Int. Conference on Boundary and Interior Layers
BAIL 2006
G. Lube, G. Rapin (Eds)
© University of Göttingen, Germany, 2006

Computation of Complex Compressible Aerodynamic Flows with a Reynolds Stress Turbulence Model

B. Eisfeld

Deutsches Zentrum für Luft- und Raumfahrt
Institut für Aerodynamik und Strömungstechnik
Lilienthalplatz 7, D-38108 Braunschweig, Germany
bernhard.eisfeld@dlr.de

1. Introduction

Aeronautical aerodynamics is characterized by compressible flows at high Reynolds numbers, so that the turbulence modeling is essential for predicting the flow field in agreement with experiments. A standard approach for this purpose is based on the so-called Reynolds-averaged Navier-Stokes (RANS) equations, where for compressible flow simple averages $\overline{\phi}$ and mass weighted averages $\widetilde{\phi}$ are distinguished. In particular the RANS momentum equation reads in tensor notation

$$\frac{\partial}{\partial t}\left(\overline{\rho}\widetilde{U}_i\right) + \frac{\partial}{\partial x_j}\left(\overline{\rho}\widetilde{U}_i\widetilde{U}_j\right) + \frac{\partial}{\partial x_j}\left(\overline{\rho}\widetilde{R}_{ij}\right) = -\frac{\partial \overline{p}}{\partial x_i} + \frac{\partial \overline{\tau}_{ij}}{\partial x_j}, \tag{1}$$

where ρ is the density, U_i the velocity vector and p is the pressure.

Usually a Newtonian fluid is considered, assuming that the viscous stress tensor keeps its mathematical form under averaging, i. e.

$$\overline{\tau}_{ij} = 2\overline{\mu}\widetilde{S}^*_{ij} = \overline{\mu}\left[\left(\frac{\partial \widetilde{U}_i}{\partial x_j} + \frac{\partial \widetilde{U}_j}{\partial x_i}\right) - \frac{2}{3}\frac{\partial \widetilde{U}_k}{\partial x_k}\delta_{ij}\right], \tag{2}$$

where μ is the dynamic viscosity of the fluid and δ_{ij} is the Kronecker tensor.

The term $\partial(\overline{\rho}\widetilde{R}_{ij})/\partial x_j$ represents the averaged contribution of the velocity fluctuations to the mean flow momentum. Searching for a suitable representation of the so-called Reynolds stress tensor $\overline{\rho}\widetilde{R}_{ij}$ in terms of mean flow quantities, i. e. mean velocity derivatives, is therefore the major focus of any RANS turbulence modelling.

The classical approach of tackling the turbulent closure problem is Boussinesq's hypothesis, assuming the same dependence of the Reynolds stresses on the traceless strain rate tensor as for the viscous stresses of a Newtonian fluid:

$$\overline{\rho}\widetilde{R}_{ij} = -2\mu^{(t)}\widetilde{S}^*_{ij} + \frac{2}{3}\overline{\rho}\widetilde{k}\delta_{ij}. \tag{3}$$

The proportionality coefficient $\mu^{(t)}$ is called eddy viscosity, the respective model class eddy viscosity turbulence models (EVM). Note, that the second term, involving the specific kinetic turbulence energy $\widetilde{k}$, is introduced for ensuring the correct trace of the Reynolds stress tensor.

There exist various types of EVMs. Algebraic or zero-equation EVMs like the Baldwin-Lomax model [1] provide the eddy viscosity directly as function of the mean flow quantities. These models usually rely strongly on the assumption of boundary layer flow and are no longer considered sufficiently accurate.

One-equation models provide a single transport equation for some quantity from which the eddy viscosity can be directly computed. In aeronautical appcliations models of the Spalart-Allmaras type [18, 4] are particularly popular.

Two-equation models usually provide one transport equation for the specific kinetic turbulence energy $\widetilde{k}$ and one for some length scale supplying variable like ϵ or ω. In aeronautical applications $\widetilde{k}$-ω models are favoured due to their superior performance in the near wall region [15]. Besides the original Wilcox model [21] the Shear Stress Transport (SST) model of Menter [14] has shown of great value for aeronautical aerodynamics due to its higher sensitvity to separation.

The major drawback of EVMs is, that the underlying assumption of the Boussinesq hypothesis, the Reynolds stress tensor being parallel to the traceless strain rate tensor, does not hold in reality. Furthermore close to walls EVMs yield isotropic normal Reynolds stresses, opposing to what is observed in measurements. Therefore a couple of deficiencies are known to occur with that type of models: The prediction of shock positions in transonic flows, the prediction of separation regions and a too rapid dissipation of free vortices with two-equation models.

Besides with the SST model [14] some improvement might be gained by so-called Explicit Algebraic Reynolds Stress Models (EARSM) like the one by Wallin and Johansson [20], particularly for the prediction of shock locations. However mathematically EARSMs take on the form of a non-linear extension of Boussinesq's hypothesis. Furthermore they rely on some background transport equations used also for EVMs, so that the gain in accuracy is restricted.

In order to overcome the described lack of accuracy and also generality of EVMs, clearly the Boussinesq hypothesis for the Reynolds stress tensor must be dropped. This is achieved by so-called differential Reynolds stress models as presented in the following.

2. The SSG/LRR-ω Differential Reynolds Stress Turbulence Model

From the momentum equation a transport equation for the Reynolds stress tensor can be derived (e. g. [22]), reading

$$\frac{\partial}{\partial t}\left(\overline{\rho}\widetilde{R}_{ij}\right)+\frac{\partial}{\partial x_k}\left(\overline{\rho}\widetilde{U}_k\widetilde{R}_{ij}\right)=\overline{\rho}P_{ij}+\overline{\rho}\Pi_{ij}-\overline{\rho}\epsilon_{ij}+\overline{\rho}D_{ij}+\overline{\rho}M_{ij}. \tag{4}$$

In this equation the production term

$$\overline{\rho}P_{ij}=-\overline{\rho}\widetilde{R}_{ik}\frac{\partial\widetilde{U}_j}{\partial x_k}-\overline{\rho}\widetilde{R}_{jk}\frac{\partial\widetilde{U}_i}{\partial x_k} \tag{5}$$

is exact, while all other terms on the right hand side need modelling.

In the EU-project FLOMANIA [8] the SSG/LRR-ω model [5, 6] has been developed, transfering the ideas of Menter's SST model [14] into the framework of differential Reynolds stress models. In particular the re-distribution term has been blended between the Launder-Reece-Rodi model (LRR) [12] near walls, omitting the so-called wall-reflexion terms as suggested by Wilcox [22], and the Speziale-Sarkar-Gatski model (SSG) [19] towards the far field. The resulting re-distribution term can be written in the following unified notation

$$\begin{aligned}\overline{\rho}\Pi_{ij} &= -\left(C_1\overline{\rho}\epsilon+\frac{1}{2}C_1^*\overline{\rho}P_{kk}\right)\widetilde{b}_{ij}\\ &\quad +C_2\overline{\rho}\epsilon\left(\widetilde{b}_{ik}\widetilde{b}_{kj}-\frac{1}{3}\widetilde{b}_{mn}\widetilde{b}_{mn}\delta_{ij}\right)+\left(C_3-C_3^*\sqrt{II}\right)\overline{\rho}\widetilde{k}\widetilde{S}_{ij}^*\\ &\quad +C_4\overline{\rho}\widetilde{k}\left(\widetilde{b}_{ik}\widetilde{S}_{jk}^*+\widetilde{b}_{jk}\widetilde{S}_{ik}^*-\frac{2}{3}\widetilde{b}_{mn}\widetilde{S}_{mn}^*\delta_{ij}\right)+C_5\overline{\rho}\widetilde{k}\left(\widetilde{b}_{ik}\widetilde{W}_{jk}+\widetilde{b}_{jk}\widetilde{W}_{ik}\right),\end{aligned} \tag{6}$$

which is formally identical with the SSG model and where $\widetilde{b}_{ij}=\widetilde{R}_{ij}/(2\widetilde{k})-\delta_{ij}/3$ is the anisotropy tensor with its second invariant $II=\widetilde{b}_{ij}\widetilde{b}_{ij}$. Note, that the specific kinetic turbulence energy is equivalent to half the trace of the specific Reynolds stress tensor, i. e. $\widetilde{k}=1/2\widetilde{R}_{ii}$.

Furthermore $\widetilde{W}_{ij} = 1/2\left(\partial\widetilde{U}_i/\partial x_j - \partial\widetilde{U}_j/\partial x_i\right)$ is the mean rotation tensor. Finally $\epsilon = C_\mu\widetilde{k}\omega$, where $C_\mu = 0.09$, and ω is provided by Menter's BSL equation [14] given further below.

The dissipation term is modeled by an isotropic tensor according to Rotta [17], reading

$$\overline{\rho}\epsilon_{ij} = \frac{2}{3}C_\mu\overline{\rho}\widetilde{k}\omega\delta_{ij}. \tag{7}$$

Simple gradient or generalized gradient diffusion models can be used alternatively, the latter being used in the applications presented below. According to [3] it reads

$$\overline{\rho}D_{ij} = \frac{\partial}{\partial x_k}\left[\left(\overline{\mu}\delta_{kl} + \widehat{D}\frac{\overline{\rho}}{\omega}\widetilde{R}_{kl}\right)\frac{\partial\widetilde{R}_{ij}}{\partial x_l}\right]. \tag{8}$$

Finally the contribution due to mass fluctuations, $\overline{\rho}M_{ij}$, is neglected, as is common practice for transonic flows.

The turbulence model is closed by Menter's BSL ω-equation [14]

$$\frac{\partial\left(\overline{\rho}\omega\right)}{\partial t} + \frac{\partial}{\partial x_k}\left(\overline{\rho}\widetilde{U}_k\omega\right) = \alpha\frac{\omega}{\widetilde{k}}\frac{\overline{\rho}P_{kk}}{2} - \beta\overline{\rho}\omega^2 + \frac{\partial}{\partial x_k}\left[\left(\overline{\mu} + \sigma\frac{\overline{\rho}\widetilde{k}}{\omega}\right)\frac{\partial\omega}{\partial x_k}\right] + \sigma_d\frac{\overline{\rho}}{\omega}\max\left(\frac{\partial\widetilde{k}}{\partial x_k}\frac{\partial\omega}{\partial x_k}; 0\right). \tag{9}$$

The blending between the SSG and the LRR regions is obtained by blending all model coefficients $\phi = C_i, C_i^*, \widehat{D}, \alpha, \beta, \sigma, \sigma_d$ between the corresponding values according to

$$\phi = F_1\phi^{(LRR)} + (1 - F_1)\,\phi^{(SSG)}, \tag{10}$$

where Menter's blending function

$$F_1 = \tanh\left(\zeta^4\right) \tag{11}$$

with

$$\zeta = \min\left[\max\left(\frac{\sqrt{\widetilde{k}}}{C_\mu\omega d}; \frac{500\overline{\mu}}{\overline{\rho}\omega d^2}\right); \frac{4\sigma^{(SSG)}\overline{\rho}\widetilde{k}}{\max\left\{2\sigma^{(SSG)}\frac{\overline{\rho}}{\omega}\frac{\partial\widetilde{k}}{\partial x_k}\frac{\partial\omega}{\partial x_k}; 10^{-20}\right\}}\right] \tag{12}$$

is used [14]. Note, that d denotes the distance from the nearest wall. The bounding values of all closure coefficients for the SSG and LRR region are given in Table 1.

	C_1	C_1^*	C_2	C_3	C_3^*	C_4	C_5	$\widehat{D}$	α	β	σ	σ_d
SSG	3.4	1.8	4.2	0.8	1.3	1.25	0.4	2.44	0.44	0.0828	0.856	1.712
LRR	3.6	0	0	0.8	0	2.0	1.11	0.5	0.5556	0.075	0.5	0

Table 1: Bounding values of closure coefficients in the SSG and the LRR region of the combined SSG/LRR-ω model.

3. Numerical Considerations

The numerical solution of the complete system of RANS equations, Reynolds stress transport equations and the length scale equation is usually considered a major challenge [13, 22] which has for a long time prevented the application of differential Reynolds stress models to industrial problems. The reasons for the numerical difficulties can be found in the mathematical properties of the equation system.

As one can see from equations (1) to (3), the RANS momentum equation of an eddy viscosity model can be written as

$$\frac{\partial}{\partial t}\left(\overline{\rho}\widetilde{U}_i\right)+\frac{\partial}{\partial x_j}\left(\overline{\rho}\widetilde{U}_i\widetilde{U}_j\right)=-\frac{\partial}{\partial x_i}\left(\overline{p}+\frac{2}{3}\overline{\rho}\widetilde{k}\right)+\frac{\partial}{\partial x_j}\left\{(\overline{\mu}+\mu^{(t)})\left[\left(\frac{\partial\widetilde{U}_i}{\partial x_j}+\frac{\partial\widetilde{U}_j}{\partial x_i}\right)-\frac{2}{3}\frac{\partial\widetilde{U}_k}{\partial x_k}\delta_{ij}\right]\right\}. \tag{13}$$

Obviously the Boussinesq hypothesis can be viewed as a redefinition of the pressure $p^*=\overline{p}+\frac{2}{3}\overline{\rho}\widetilde{k}$ and the viscosity $\mu^*=\overline{\mu}+\mu^{(t)}$. Whereas the pressure modification is usually considered negligible, the eddy viscosity exceeds the molecular viscosity in a boundary layer by an order of magnitude. Thus the eddy viscosity enhances the damping effect of the second derivatives of the velocities and hence stabilizes the numerical solution.

In contrast, with a differential Reynolds stress model the RANS momentum equation keeps the form of equation (1), where the Reynolds stresses enter via a divergence term. These first derivatives tend to destabilize the numerical solution, while at the same time the stabilizing influence of an eddy viscosity is missing. Furthermore the Reynolds stress transport equation (4) is dominated by the source terms of the right hand side, where the abbreviating tensor notation of equations (5) and (6) hides the true number of individual contributions. Therefore it is virtually impossible to *ad hoc* separate stabilizing and destabilizing terms, as might be done with one- or two-equation models.

For solving the problem, a detailed stability analysis of the complete system of RANS equations, Reynolds stress transport equations and the length scale equation has been carried out. As it comes out, the spectral radius has to be altered to $\lambda_{max}=\sqrt{\widetilde{a}^2+2\widetilde{k}}$, where $\widetilde{a}$ denotes the speed of sound. Furthermore the production and re-distribution terms (5) and (6) are carefully linearized, in order to allow properly for an implicit integration scheme. As will be demonstrated below, these measures indeed lead to a robust and efficient numerical method, that is applicable to industrial aeronautical flow problems up to very high complexity.

4. Applications

In the EU-project FLOMANIA [8] the SSG/LRR-ω model has been implemented into DLR's block-structured flow solver FLOWer [16], that is based on a central second order space discretizaton with artificial dissipation [9] for the RANS equations and a first order upwind discretization for the turbulence equations.

The RANS equations are integrated by an explicit hybrid five-stage Runge-Kutta method, that is accelerated by local time stepping, implicit residual smoothing and multigrid [10], whereas the turbulence equations are integrated by a DDADI scheme on the finest grid level only, which has proven to be robust with one- and two-equation models [7].

The implementation has been validated and the robustness of the numerical method has been proven for a wide variety of test cases, some of which are presented in the following.

4..1. A-310 Airfoil in Landing Configuration

The A-310 airfoil in landing configuration consists of a main airfoil with deflected slat and flap and has been used as test case in the EU-projects EUROLIFT and EUROLIFT-II investigating high-lift flow. The computations were carried out at a subsonic Mach number of 0.22 and a Reynolds number of $4.1\cdot10^6$, where the angle of attack was varied from the linear range until lift break down. The grid consisted of 84000 cells distributed to 9 blocks, where the wall-normal spacing satisfied the requirements for an appropriate resolution of the viscous sublayer.

As on can see in Figure 1, rather good agreement with the measured polar is achieved by the SSG/LRR-ω model, while EVMs as the Menter SST show an overshoot and too massive lift break down.

4..2. LANN Wing

The LANN wing has been mainly used for studying unsteady flows [23], nevertheless there exist a couple of steady measurements. Out of these the so-called test case CT9 (Mach number 0.82, Reynolds number $7.17 \cdot 10^6$, incidence 2.6^0) is of particular interest, because of a shock induced separation bubble extending over large parts of the wing span. The test case has been computed on a grid, consisting of $4.3 \cdot 10^3$ cells, distributed to 4 blocks which is fine enough to achieve a grid independent solution.

Figure 2 shows the pressure distributions at 47.5% span obtained with the SSG/LRR-ω and two k-ω models. Clearly the Reynolds stress model solution is in fair agreement with the experiments, whereas the Wilcox k-ω model predicts the shock too far downstream, because it underestimates the separation. In contrast, the SST model overpredicts the separation bubble, so that the pressure distribution is completely off.

4..3. DLR-F6 Generic Aircraft

The DLR-F6 generic aircraft model, depicted in Figure 3, has been selected as test case for the 2nd AIAA Drag Prediction Workshop [11], where polar computations were carried out at a Mach number of 0.75 and a Reynolds number of $3 \cdot 10^6$. Figure 4 shows the polar obtained on the medium workshop grid, consisting of $8.3 \cdot 10^6$ cells distributed to 62 blocks. Note, that on the abscissa the induced drag has been subtracted from the total drag (aspect ratio $\Lambda = 9.5$). This test case not only demonstrates the applicability of the SSG/LRR-ω model to flows around complex aircraft configurations, but also reveals its good predictive capabilities. Note, that despite the observed deviations the agreement with the experiments is considered very good.

4..4. Dauphin Helicopter Fuselage

Another example, demonstrating the general applicability of differential Reynolds stress models to complex configurations, is the flow around the Dauphin helicopter fuselage depicted in Figure 5. This test case has been investigated in the German/French cooperation CHANCE on helicopter aerodynamics. ONERA has provided the grid, consisting of $6.8 \cdot 10^6$ cells distributed to 97 blocks, where the flow is characterized by a Mach number of 0.0441, a Reynolds number of $1.074 \cdot 10^6$ and an incidence of -3^0.

There are only few pressure measurements available for this flow which are difficult to interpret. Therefore mainly the resolution of vortices occurring in the flow field has been studied. Figure 6 shows a front view of the skin friction distribution and skin friction lines on the engine casing and upper fuselage predicted wih the SSG/LRR-ω model. Compared to a two-equation EVM (not presented here), the former resolves the formation of the vortex at the intersection between the engine casing and the fuselage in much more detail and keeps it much stronger downstream.

5. Conclusions

Appropriate turbulence modelling is essential for accurate predictions of complex aeronautical flows. Eddy viscosity models, although currently widely used, suffer from the deficiencies of the underlying Boussinesq hypothesis. This assumption is abandoned, when using differential Reynolds stress turbulence models.

In the EU-project FLOMANIA the SSG/LRR-ω model has been developed, transferring the ideas of Menter's well-known SST model into the framework of Reynolds stress modelling. No particular numerical difficulties are encountered with that model even in complex industrial applications, when using a modified spectral radius and a careful linearization of the turbulence equations in conjunction with an implicit integration scheme.

The SSG/LRR-ω model performs well in various flow situations, including high-lift flow, flows with three-dimensional shock induced separation and complex transonic and subsonic aircraft flow. Depending on the test case and the reference model, the Reynolds stress model requires 1.5 to 2 times more CPU time per iteration and twice the memory of a two-equation eddy viscosity model which is considered acceptable.

The SSG/LRR-ω model is currently transfered to DLR's unstructured flow solver TAU, where first results confirm the robustness of the numerical method observed with DLR's structured FLOWer code.

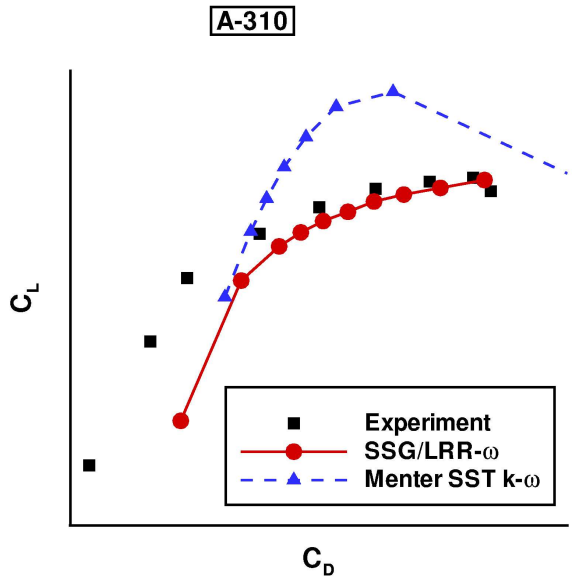

Figure 1: A-310 airfoil. Polar for landing configuration.

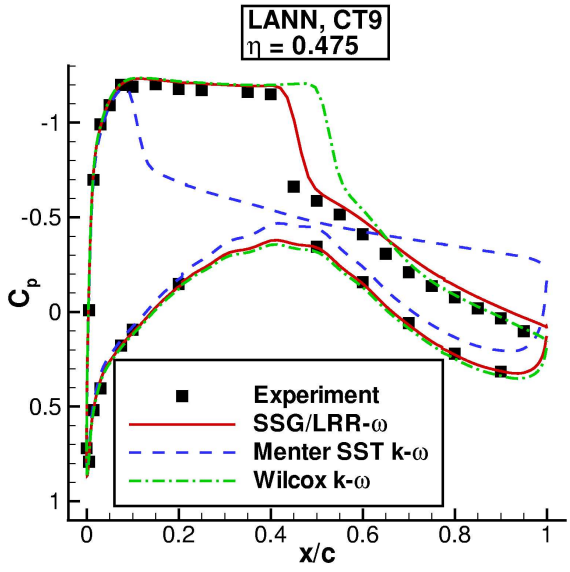

Figure 2: LANN wing. Pressure distributions for test case CT9 at 47.5% span.

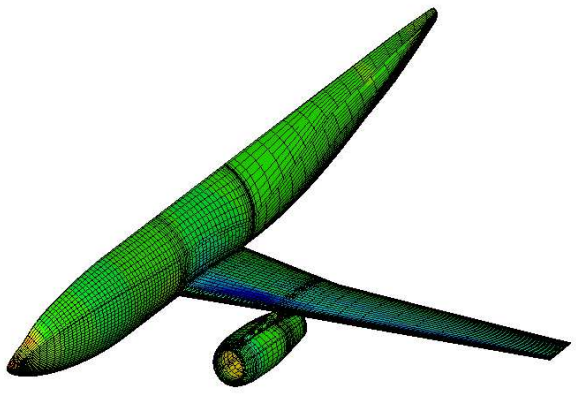

Figure 3: DLR-F6 generic aircraft. Geometry of the half model (2nd grid level).

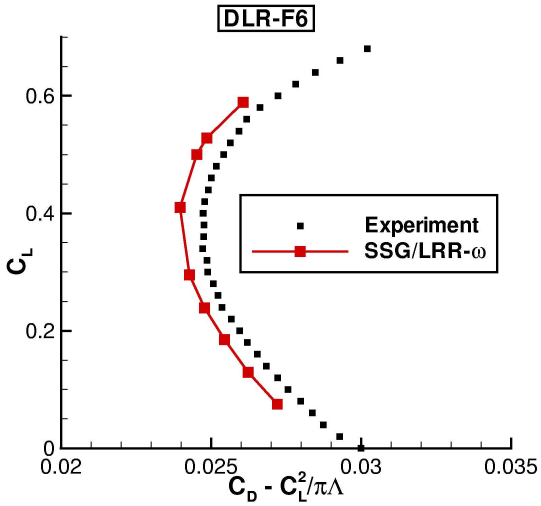

Figure 4: DLR-F6 generic aircraft. Polar.

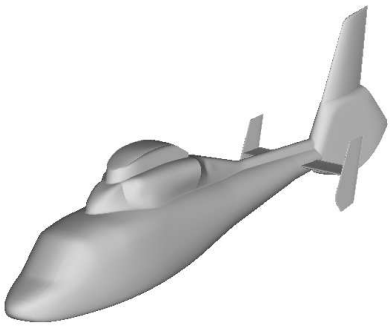

Figure 5: Dauphin helicopter fuselage (full model).

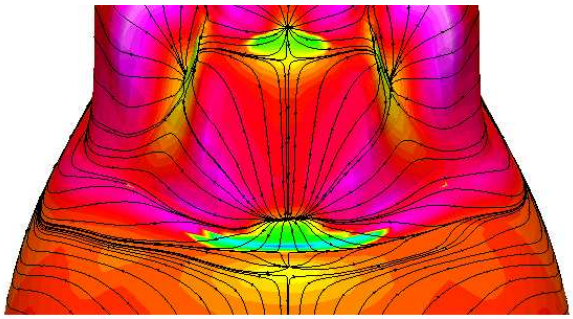

Figure 6: Dauphin, front view on engine casing/fuselage intersection. Skin friction prediction by SSG/LRR-ω model.

References

[1] Baldwin, B. S., Lomax, H., Thin Layer Approximation and Algebraic Model for Separated Turbulent Flows, *AIAA-Paper 78-0257*, 1978

[2] Cook, P. H., McDonald, M. A., Firmin, M. C. P., Aerofoil RAE 2822 – Pressure Distributions, and Boundary Layer and Wake Measurements. In: J. Barche (Ed.), *Experimental Data Base for Computer Program Assessment*, AGARD-AR-138, 1979

[3] Daly, B. J., Harlow, F. H., Transport equations of turbulence, *Physics of Fluids* **13** (1970) 2634-2649

[4] Edwards, J. R., Chandra, S., Comparison of Eddy Viscosity–Transport Turbulence Models for Three-Dimensional, Shock-Separated Flowfields, *AIAA Journal*, **34** (1996) 756-763

[5] Eisfeld, B., *Implementation of Reynolds stress models into the DLR-FLOWer code*, DLR-Institutsbericht, DLR-IB 2004-31, 2004

[6] Eisfeld, B., Brodersen, O., Advanced Turbulence Modelling and Stress Analysis for the DLR-F6 Configuration, *AIAA-Paper 2005-7727*, 2005

[7] Fassbender, J. K., *Improved Robustness for Numerical Simulation of Turbulent Flows around Civil Transport Aircraft at Flight Reynolds Numbers*, DLR-Forschungsbericht, DLR-FB 2003-09, 2004

[8] Haase, W., Aupoix, B., Bunge, U., Schwamborn, D. (Eds.), *FLOMANIA – A European Initiative on Flow Physics Modelling*, Notes on Numerical Fluid Mechanics and Multidisciplinary Design, Vol. 94, to appear 2006

[9] Jameson, A., Schmidt, W., Turkel, E., Numerical solutions for the Euler equations by finite volume methods using Runge-Kutta time-stepping schemes, *AIAA Paper 81-1259*, 1981

[10] Kroll, N., Eisfeld, B., Bleecke, H. M., FLOWer. In: Schüller, A. (Ed.), *Portable Parallelization of Industrial Aerodynamic Applications (POPINDA)*, Notes on Numerical Fluid Mechanics, Vol. 71, Vieweg, 1999, pp. 55-71

[11] Laflin, K., Klausmeyer, S. M., Zickuhr, T., Vassberg, J., Wahls, R., Morrison, J., Brodersen, O. P., Rakowitz, M. E., Tinoco, E. N., Godard, J. L., Data Summary from Second AIAA Computational Fluid Dynamics Drag Prediction Workshop, *AIAA Paper 2004-0555*, 2004

[12] Launder, B. E., Reece, G. J., Rodi, W., Progress in the development of a Reynolds-stress turbulence closure, Journal of Fluid Mechanics, **68** (1975) 537-566

[13] Leschziner, M. A., Lien, F.-S., Numerical Aspects of Applying Second-Moment Closure to Complex Flows. In: Launder, B., Sandham, N. (Eds.), *Closure Strategies for Turbulent and Transitional Flows*, Cambridge University Press, 2002, pp. 153-187

[14] Menter, F. R., Two-Equation Eddy-Viscosity Turbulence Models for Engineering Applications, *AIAA Journal*, **32** (1994) 1598-1605

[15] Menter, F. R., Kuntz, M., Langtry, R., Ten Years of Industrial Experience with the SST Turbulence Model. In: Hanjalić, K., Nagano, Y., Tummers, M. (Eds.), *Turbulence, Heat and Mass Transfer 4*, Begell House, 2003, pp. 625-632

[16] Raddatz, J., Fassbender, J. K., Block Structured Navier-Stokes Solver FLOWer. In: Kroll, N., Fassbender, J. K. (Eds.), *MEGAFLOW - Numerical Flow Simulation for Aircraft Design*, Springer, 2005, pp. 27-44

[17] Rotta, J., Statistische Theorie nichthomogener Turbulenz, *Zeitschrift für Physik*, **129** (1951) 547-572

[18] Spalart, P. R., Allmaras, S. R., A one-equation turbulence model for aerodynamic flows, *La Recherche Aérospatiale*, **1** (1994) 5-21

[19] Speziale, C. G., Sarkar, S. Gatski, T. B., Modelling the pressure-strain correlation of turbulence: an invariant dynamical systems approach, Journal of Fluid Mechanics, **227** (1991) 245-272

[20] Wallin, S. Johansson, A. V., An explicit algebraic Reynolds stress model for incompressible and compressible turbulent flows, *Journal of Fluid Mechanics*, **403** (2000) 89-132

[21] Wilcox, D. C., Reassessment of the Scale-Determining Equation for Advanced Turbulence Models, *AIAA Journal*, **26** (1988) 1299-1310

[22] Wilcox, D. C., *Turbulence Modeling for CFD*, DCW Industries, La Cañada, USA, 2nd ed., 1998

[23] Zwaan, R. J., LANN Wing, Pitching Oscillation. In: Lambourne, N. C. (Ed.), *Compendium of Unsteady Aerodynamic Measurements*, AGARD-R-702 Addendum No. 1